IEEE Access
Multidisciplinary | Rapid Review | Open Access Journal

Received July 21, 2019, accepted September 13, 2019, date of publication September 20, 2019, date of current version October 4, 2019.

Digital Object Identifier 10.1109/ACCESS.2019.2942722

Acoustic Standing Wave Field Measurement Using a Laser Doppler Vibrometer Based on the Hankel Fourier Algorithm

HUIJUAN DONG[1], ZHEN YU[1], KENNETH THOMAS VICTOR GRATTAN[2], TONG SUN[2], AND TIANLONG LI[1,3]

[1]State Key Laboratory of Robotics and Systems, Harbin Institute of Technology, Harbin 150001, China
[2]School of Mathematics, Computer Science and Engineering, City University of London, London EC1V 0HB, U.K.
[3]Institute of Pharmacy, Sechenov University, 119991 Moscow, Russia

Corresponding author: Huijuan Dong (dhj@hit.edu.cn)

This work was supported by the National Natural Science Foundation of China under Grant 51675140 for Huijuan Dong.

ABSTRACT Measuring the acoustic pressure in an acoustic standing wave field is essential as a means to study acoustic levitation and other related techniques. In this work it was shown that the pressure of an acoustic standing wave field could be measured on line, in a non-contact way, using a scanning Laser Doppler Vibrometer (LDV), where the LDV output is proportional to the integral of the acoustic pressure over the laser path. In the method used to measure acoustic pressure, first, the LDV outputs, υ_{sLDV} and υ_{eLDV}, are obtained by using both COMSOL-MATLAB-based (CM) co-simulation and through experimental measurements. Next, the acoustic pressure distribution is obtained using a MATLAB-based programme and this is reconstructed by using υ_{sLDV} and υ_{eLDV}, based on the Hankel-Fourier (HF) algorithm. Further, the acoustic pressure measurements obtained by using these two methods are cross compared, in that way to demonstrate the effectiveness of the method presented.

INDEX TERMS Acoustic standing wave field, acoustic pressure measurement, laser Doppler vibrometer (LDV), LDV output, Hankel-Fourier (HF) algorithm, COMSOL-MATLAB-based co-simulation.

I. INTRODUCTION

Acoustic technology developed rapidly in recent years [1]–[5] and especially acoustic levitation, which has a further, broad application in several areas of technology, including material preparation and treatment [6]–[8], biological research [9]–[13], chemical analysis [14]–[16] and droplet dynamics [17]–[19] while pressure measurement in an acoustic field is essential in research into acoustic levitation.

The LDV-based acoustic pressure measurement method is favored because of its high resolution and lack of interference to the acoustic field. In recent years, significant progress into underwater acoustic pressure measurement using LDV has been made. For example, Wang *et al.* [20] used LDV to measure the velocity of particles in water but, however, they did not obtain the acoustic pressure distribution in the area over which they made measurements. Lerch and Chen *et al.* [21], [22] used LDV to measure the underwater acoustic pressure and even obtained data on the variation of acoustic pressure in water and transparent solids, as a function of time. The rapid progress in LDV-based underwater acoustic measurement is possible because of the strong acousto-optic effect of liquids and solids, a subject which has been extensively studied [23]. By contrast, the method which is used to measure the acoustic pressure in air made rather more slow progress. Nakamura *et al.* [23] first used LDV to measure the acoustic pressure distribution of a uniform acoustic field and following that both Koyama and Nakamura [24] in Japan and Marco in Brazil [25]–[27] used this method to measure the acoustic field in air, during their acoustic levitation experiments. However, they only used the LDV output (υ_{LDV}) rather than the acoustic pressure distribution, which they did not obtain. In other research, Antoni *et al.* [28], Efren *et al.* [29], Antoni [30] deduced the theoretical formulation for acoustic field measurement using LDV, where they reconstructed a 2kHz acoustic field generated by a loudspeaker using the velocity output and an inverse Radon transformation. Contrasting with that approach, in this work

The associate editor coordinating the review of this manuscript and approving it for publication was Jiansong Liu.

the relationship between the harmonic acoustic pressure and the corresponding LDV velocity output caused by nonlinearity is considered. At the same time, taking into account that the shape of acoustic pressure of a single-axis acoustic levitation is usually axisymmetric, a different algorithm was used specifically to reconstruct the acoustic field, i.e. the Hankel-Fourier (HF) transform. It is noteworthy that Ishikawa *et al.* [31] even achieved high-speed imaging of propagating sound waves using parallel phase-shifting interferometry (PPSI) with a high-speed polarization camera.

Specifically in this work, harmonic generation [25] is taken into account in a method described by the authors, which is used to measure acoustic pressure distribution in an axisymmetric acoustic field. First, the simulated LDV output, v_{sb} and the experimental velocity output v_e, are COMSOL-MATLAB-based (CM) co-simulated and also experimentally obtained. Next, the acoustic pressure p_{rs} and p_e are reconstructed by using the values of v_{sb} and v_e respectively. Finally, the reconstructed acoustic pressure is compared with the acoustic pressure p_s obtained using COMSOL simulation.

II. METHOD USED TO MEASURE ACOUSTIC PRESSURE USING LDV

A. THE RELATIONSHIP BETWEEN ACOUSTIC PRESSURE AND V_{LDV}

LDV is often used to measure the surface vibration of solid or fluid flow [32], utilizing the Doppler frequency shift. Specifically, LDV is also used to measure the acoustic pressure in air due arising from the acousto-optic effect where the acoustic pressure can change the air refractive index and the principle of measuring acoustic pressure using LDV is illustrated in Fig.1.

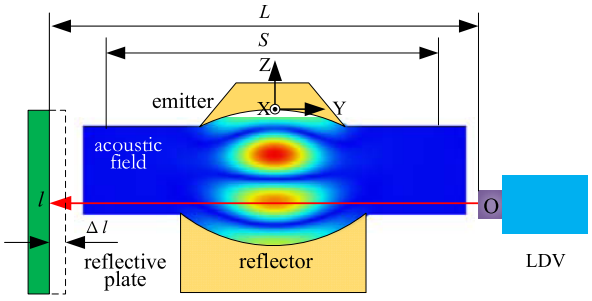

FIGURE 1. Principle of LDV-based acoustic measurement.

When the laser used for the LDV experiments irradiates a fixed reflective plate and the reflective plate is not moving, then $v_{LDV} = 0$. When the laser beam passes through an acoustic field, the acoustic pressure will change the refractive index, n, of the air in this region. The variation of n can be equivalent not only to a variation of Δl but also to a variation in v_{LDV}.

When the laser beam in the LDV experiment passes through an acoustic field, with constant acoustic pressure amplitude P, then v_{LDV} can be written as [23]:

$$v_{LDV} = \frac{2\pi f}{c_0^2 \rho_0} \cdot \frac{n-1}{n} PS$$

where c_0, ρ_0 represent speed of sound in air and the air density respectively. S is the distance over which the laser light overlaps with acoustic pressure field and the emitter frequency is f.

Here the emitter or the reflector of the levitator developed are formed into a spherical surface, and thus the acoustic pressure is no longer constant, rendering the formula above not suitable. Alternatively, a coordinate system is established, as shown in Figure 1, where the variation of the refractive index $\Delta n(l, t)$ can be seen as equivalent to the virtual displacement of the reflective plate $\Delta l(t)$ and thus:

$$\int_0^L \Delta n(l,t) dl = n \cdot \Delta l(t),$$

The derivative of t on both sides of the equation can be described by:

$$\int_0^L \frac{d\Delta n(l,t)}{dt} dl = n \cdot v_{LDV}(t), \tag{1}$$

The relationship between the variation of air refractive index and the volume change rate is given by:

$$\frac{\Delta V(l,t)}{V} = -\frac{\Delta n(l,t)}{n-1}, \tag{2}$$

The acoustic field formulation is satisfied as follows:

$$\frac{p(l,t)}{P_0} = -\gamma \frac{\Delta V(l,t)}{V}, \tag{3}$$

$$P_0 \gamma = c_0^2 \rho_0, \tag{4}$$

where P_0 is the absolute pressure of atmosphere, γ is the ratio of the two specific heats, $p(l, t)$ is the acoustic pressure at a location of l and a time of t. $v_{LDV}(t)$ can be obtained when equations (2), (3) and (4) are substituted into equation (1):

$$v_{LDV}(t) = \frac{1}{c_0^2 \rho_0} \cdot \frac{n-1}{n} \int_0^L \frac{dp(l,t)}{dt} dl \tag{5}$$

As the acoustic pressure periodically changes in a sine (or cosine) mode, and harmonics will be generated within a high intensity acoustic field [25], then $p(l, t)$ can be given by:

$$p(l,t) = \sum_{m=1}^{\infty} p_m(l) \cos(2m\pi f t + \varphi_m(l)), \tag{6}$$

where $m = 1, 2, 3\ldots$, $p_{\mathrm{m}}(l)$ is the acoustic pressure amplitude for the m^{th} harmonic at l. $v_{LDV}(t)$ can be rewritten as:

$$v_{LDV}(t) = m \cdot \eta \int_0^L \sum_{m=1}^{\infty} p_m(l) \sin(2m\pi f t + \varphi_m(l)) dl, \tag{7}$$

where $\eta = \frac{2\pi f}{c_0^2 \rho_0} \cdot \frac{n-1}{n}$,

When a standing wave is formed in an acoustic field, the amplitude of υ_{mLDV} corresponding to each harmonic can be expressed approximately as:

$$\upsilon_{mLDV}(t) = m \cdot \eta \int_0^L p_m(l) \sin(2m\pi ft + \varphi_m(l))dl, \quad (8)$$

It is known from equation (8) that $\upsilon_{LDV}(t)$ is proportional to the integral of the acoustic pressure over the laser beam path, L. Furthermore, the influence of the harmonic generation on υ_{LDV} is taken into account, which was not considered in previous work reported in the literature [23], [25]. It should be noted that only the relationship between υ_{LDV} fundamental component υ_{bLDV} and acoustic pressure fundamental component p_b are verified in this work.

B. RECONSTRUCTION OF AN ACOUSTIC FIELD USING HF ALGORITHM

The pressure of an axisymmetric acoustic field can be calculated using the HF algorithm according to υ_{LDV} [33], [34]. This process has been termed acoustic field reconstruction by the authors. In general, as the emitter and reflector of a levitator are kept along a central axis, an axisymmetric acoustic pressure distribution is generated where the structural parameters of the levitator developed are shown in Fig.2.

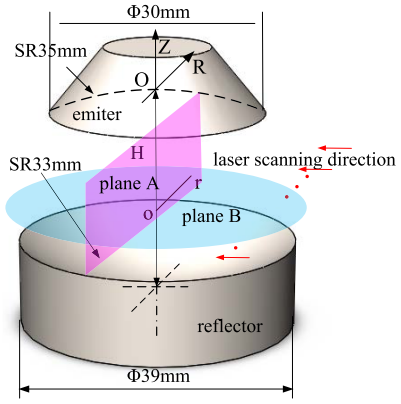

FIGURE 2. Structural parameters of the levitator.

Circular plane B is one of the measured planes, as is also the plane of the incident laser beam, which is perpendicular to plane A and the intersection in the r axis. Furthermore, plane A passes through the Z-axis.

The relationship between the acoustic pressure at plane B and υ_{LDV} is shown in Fig.3. In order to obtain the distribution of the acoustic pressure on plane B, this plane is divided into successive rings, of width increment Δr. Thus it can be visualized that the (N+1) laser beam elements pump along the inner boundary of each ring, in parallel, as shown in Figure 3. It is noted that the acoustic pressure distribution is symmetric about the center, thus the laser scanning direction can be in any direction.

It is known that the LDV output $\upsilon_{LDV}(i\Delta r)$ can be expressed using the curve shown in Fig.3 when the plane B

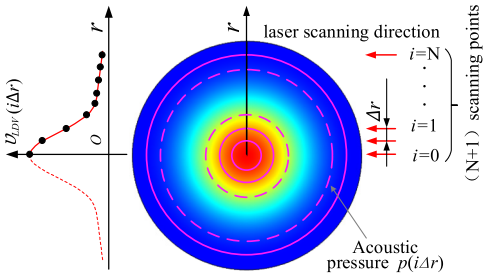

FIGURE 3. Relationship between acoustic pressure of plane B and V_{LDV}.

is monitored, responding to equation (8). It is important to note that L refers to the border of plane B, which means that $\upsilon_{LDV}(i\Delta r)$ can be obtained by a knowledge of the acoustic pressure, $p(i\Delta r)$ and the border of the plane B in the acoustic field. In other words, the acoustic pressure, $p(i\Delta r)$ can also be calculated using $\upsilon_{LDV}(i\Delta r)$ and the position of the border of the acoustic field. This method of acoustic pressure calculation is termed the reconstruction of the acoustic field in this work.

Further, $p(r)$ of plane B can be expressed [33], [34]:

$$p(r) = \frac{1}{2\pi} HaT^{-1}[R(u)] = \frac{1}{2\pi} \int_0^{+\infty} R(u) \cdot u \cdot J_0(ru)du$$

where, u is spatial frequency,
$u = \frac{2N+1}{r}$, $\Delta u = -\frac{2N+1}{r^2}\Delta r$, $\Delta r = \frac{r}{2N+1}$.
$R(u)$ is the spatial Fourier transform.
$R(u) = FT[\frac{\upsilon_{LDV}(r)}{\eta}] = \int_{-\infty}^{+\infty} \frac{\upsilon_{LDV}(r)}{\eta} e^{-jru}dr$.
$J_0(\cdot)$ is the zero Bessel function.
$HaT^{-1}[\cdot]$ represents the inverse Hankel transform.
$p(r)$ of plane B which can be written.

$$\begin{aligned} p(r) &= \frac{1}{2\pi} \int_0^{+\infty} [\int_{-\infty}^{+\infty} \frac{\upsilon_{LDV}(r)}{\eta} e^{-jru}dr] \cdot u \cdot J_0(ru)du \\ &= \frac{1}{2\pi} \int_0^{+\infty} [\int_{-\infty}^{+\infty} \frac{\upsilon_{LDV}(r)}{\eta} \cos(ru)dr] \cdot u \cdot J_0(ru)du \end{aligned}$$

Therefore,

$$\begin{aligned} p(i\Delta r) = &\frac{1}{\eta 2\pi (2N+1)^2 \Delta r} \sum_{m=-N}^{N} \\ &\times \left\{ \upsilon_{LDV}(m\Delta r) \sum_{k=0}^{N} [\cos(\frac{mk}{2N+1}) k J_0(\frac{ik}{2N+1})] \right\} \end{aligned} \quad (9)$$

where i varies from 0 to N, $\upsilon_{LDV}(m\Delta r)$ is measured using LDV at the position $m\Delta r$, and thus the acoustic pressure within the acoustic field can be obtained. υ_{LDV} which is obtained can be used to calculate the acoustic pressure, according to equation (9), this being termed the HF-based reconstruction of the acoustic field in this work.

It is noted that m is the number of LDV laser scanning points and $2N + 1 = 121$ in this work. In order to calculate the pressure at the position $i\Delta r$ in plane B, $\upsilon_{LDV}(m\Delta r)$ is written as a full matrix C of size 1×121. As the radius of

the plane B is 30mm and $\Delta r = 0.5mm$, $N = \frac{r}{\Delta r} = 60$. $\sum_{k=1}^{N} [\cos(\frac{mk}{2N+1}) \cdot k \cdot J_0(\frac{ik}{2N+1})]$ can be rewritten as a matrix D of size 121×1. Therefore, the pressure at $i\Delta r$ can be obtained using matrices C by D thus developed.

III. EXPERIMENTAL SET-UP

In the experiment set up, the acoustic field was generated between the emitter and the reflector by using the Langevin-type transducer developed, at a frequency of 21033Hz. All the structural parameters are shown in Fig.2. The distance between the reflector and the emitter is given by H where the transducer is powered using a power supply developed for it.

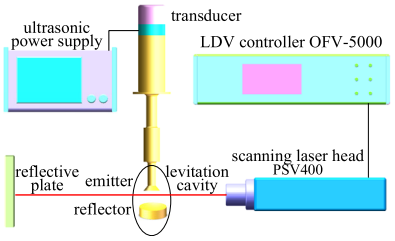

FIGURE 4. Schematic of the experimental set-up used in this work.

A schematic of the experimental set-up is shown in Fig.4. H is adjusted by using the electrical actuator (Harmonic, Japan) using C#-programming with a step size of $3\mu m$ to achieve the third mode, during the experiments. The LDV system (Polytec, Germany) comprises a PSV400 Scanning Head and an OFV-5000 controller. The corresponding software used with the LDV are PSV Acquisition for the basic measurements and PSV Presentation for the data processing. As a result, υ_{LDV} from the PSV400 Scanning Head is Fast Fourier transformed to υ_{bLDV} (without needing to develop further specific software). υ_{bLDV} is equivalent to the velocity of the reflective plate and this satisfies the relationship in equation (9). Although the PSV400 Scanning Head could not be moved, the $(2N + 1)$ scanning laser beams considered are approximately parallel, due to the fact that the distance between the Head and the measured acoustic field is much greater than that between the reflective plate and the acoustic field. The spacing distance between the two adjacent scanning laser beam elements is $\Delta r = 0.5mm$ (where this can be calibrated using the mesh on the reflective plate).

IV. EXPERIMENTS AND SIMULATIONS

A. υ_{eb} DISTRIBUTION MEASUREMENT AT SERIES OF LEVITATION MODES

During the experiment, the LDV set up was used to measure υ_{LDV} along a plane where Z= -9mm (where the pressure reaches the peak), and recorded as $\upsilon_{eb.}$ It is noted that υ_{eb} is obtained by experimental measurement and the acoustic pressure is calculated using the value of υ_{eb}, and recorded as p_{re}. Meanwhile, υ_{sb} is obtained by simulation and the acoustic pressure is calculated using υ_{eb}, recorded as υ_{sb}. By changing H until the maximum value of υ_{eb} is used, the levitation modes from the 2nd to the 5th are found when H has values of 19.04 mm, 27.94 mm, 36.84 mm and 45.50 mm, which are well suited to the simulations carried out.

The longitudinal distribution of υ_{eb} at each levitation mode is shown in Figure 5. It should be noted that red colored part in the figure indicates a large value of $\upsilon_{eb.}$ and its shape is similar to that of the acoustic pressure.

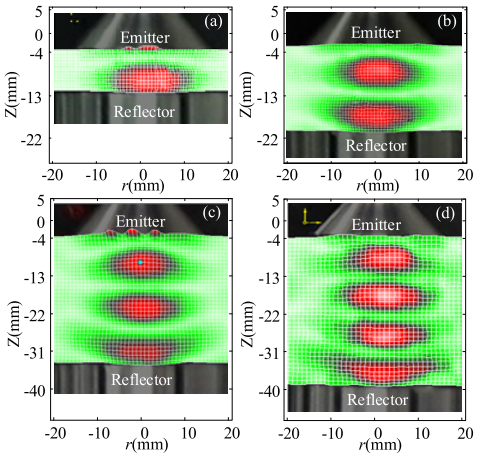

FIGURE 5. υ_{eb} distribution at each levitation mode, f =21033Hz, the distances between the emitter and the reflector are 19.04mm, 27.94mm, 36.84 mm and 45.50mm respectively. Graphs (a) to (d) are the 2nd, the 3rd, the 4th and the 5th levitation mode respectively.

B. COMPARISON OF υ_{SB} with υ_{eb}

The acoustic pressure at the 3th levitation mode, p_s, is obtained by using the COMSOL-based program in this section. When υ_{sb} is calculated using p_s, (which is in accordance with equation (8) ($m = 1$)), finally, υ_{sb} and υ_{eb} are compared under the conditions where all the experimental parameters are set to be directly comparable with those in the simulations, to allow a close comparison to be made.

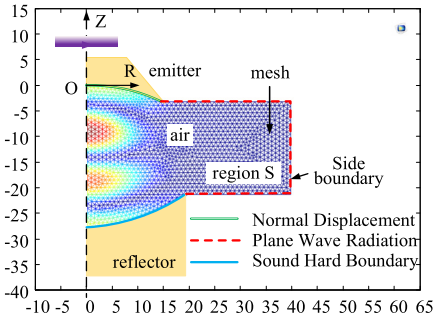

FIGURE 6. Schematic of the acoustic pressure simulation in the axisymmetric acoustic field.

As shown in Figure 6, only the right hand side (region S) need be simulated in this work (due to the symmetrical distribution of the acoustic pressure). Here the emitter surface is the Normal Displacement A_0, the reflector surface is the Sound Hard Boundary and the side boundary is the Plane

TABLE 1. The parameters set during the simulation.

Parameter name	Value	Units
H	27.815	mm
Vibration frequency of the emitter f	21033	Hz
Vibration amplitude of the emitter A_0	0.4	μm
Sound speed c_0 in air	340	m/s
Refractive index of air n	1.00027	-
Density of air ρ	1.2	kg/m^3
Radius of the boundary R_l	40	mm

Wave Radiation. The parameters set during the simulation are shown in Table 1. Since the vibration amplitude of the emitter surface is 0.396μm in the actual measurement, this parameter in the simulation is set to 0.4μm, to match with the experiment. The acoustic pressure distribution for other vibration amplitudes can be acquired just by multiplying the corresponding constant with the acoustic pressure distribution obtained here [25].

It is known from equation (8) that v_{bLDV} can be approximately calculated as follows:

$$v_{bLDV} = \eta \int_0^L p_b(l)dl, \tag{10}$$

where $p_b(l)$ is an acoustic pressure amplitude at location, l in the scanning plane A. Plane A is scanned 81 times in the R direction, due to it being 40mm in length (with a 0.5mm spacing). Meanwhile, it is scanned 36 times in the Z direction (due to it being 18mm in height with again a 0.5mm spacing). The three-dimensional acoustic pressure $p_b(l)$ is obtained by rotating the acoustic field, shown in Fig.6, which is saved in a file (type aspr.absp in the MATLAB-COMSOL-based simulation program). The integral of $p_b(l)$ is achieved by using a function in COMSOL. L is the boundary of the measured acoustic field, which is distinguished automatically in the program. The v_{sb} distribution along the longitudinal section of the acoustic field is shown in Figure 7(a), where here H is shown in the third levitation mode.

The distribution of v_{eb} on the same longitudinal section is obtained by experiments carried out where the emitter vibrates at an amplitude of 0.396μm. The laser pumps through and strikes vertically plane A, as shown in Fig.2 where here the reflective plate is chosen as the reference plane. The scanning mesh is drawn on on the reference plane and the laser beam is made to focus at each point automatically. The v_{eb} distribution, shown in Figure 7(b), can be obtained directly since the experimental software PSV has the ability to carry out a FFT (Fast Fourier Transform). It can be seen that the experimental results obtained match well with those from the simulation, in terms of the overall shape and other details of the results obtained.

In order to verify the degree of fit between the simulation and experimental results, they are compared at four representative cross section values (i.e. along plane B at different

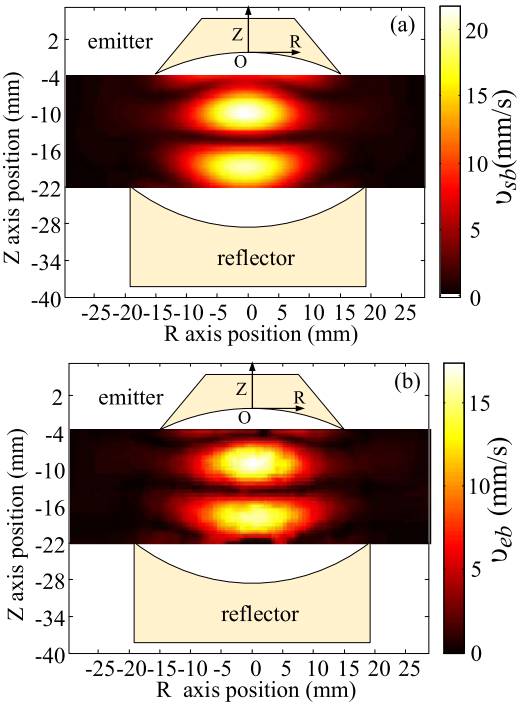

FIGURE 7. v_{bLDV} **distribution on the longitude section of the acoustic field at the 3rd levitation mode, (a) the simulation result, (b) the experimental result.**

locations) in the acoustic field. In Figure 7(b), it can be seen that v_{eb} reaches its maximum around values of Z= −9.5mm and R=0. The minima appear at Z= −5.5mm, Z= −14mm, Z= −22.5 and R=0, termed the acoustic pressure nodes. As a result, two typical planes where Z= −9.5 and Z= −5.5 are used by the authors for cross comparison.

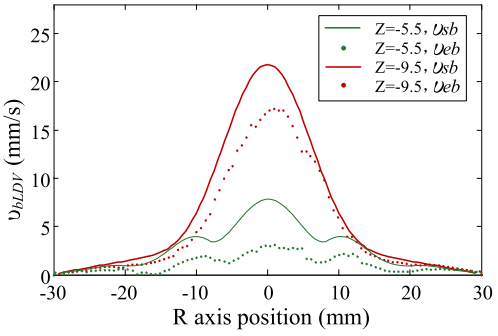

FIGURE 8. v_{bLDV} **comparison between the simulation and the experiment on the two typical cross sections.**

As shown in Figure 8, the dotted and continuous lines represent the experimental and simulation values of v_{bLDV}. Respectively, where it can be seen that both are similar in shape, but deviate to a certain extent one from the other. In fact, it is difficult to achieve a very close match between the simulation and the experimental results, for the following reasons. The parameters used in the simulation and experimental parameters are not exactly the same as the simulation

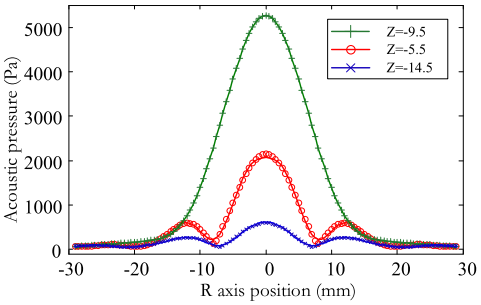

FIGURE 9. The comparison between the HF-based reconstructed p_{rs} and COMSOL simulated p_s.

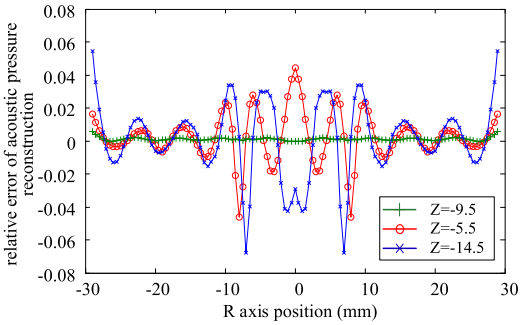

FIGURE 10. Relative error between reconstruction and simulation acoustic pressure.

is carried out under ideal conditions: such as not considering factors such as the air friction, temperature and several other physical factors. The term c_0^2 in equations (7) and (9) shows that the calculated result for the acoustic pressure would be sensitive to even a small variations in c_0^2. Generally, the sound speed will increase by 3m/s as the temperature increases by 5°C and the corresponding acoustic calcualtion result would then deviate by 1.8%, which illustrates how the acoustic pressure is sensitive to temperature changes not taken into account in the model. The simplification of the experimental set up for the simulation, for instance, where the phase of the acoustic pressure along the laser path is considered to be same and the scanning laser beam is assumed to be parallel reflect the differences in the two sets of results. Other factors not taken into account in the simulation, such as acoustic streaming, may also affect the comparison with the experimental results.

C. ACOUSTIC FIELD RECONSTRUCTION BASED ON HF ALGORITHM

The acoustic field is reconstructed based on the HF algorithm in this work by using υ_{sb} from the simulations and υ_{eb} from the experimental results, in order to verify the effectiveness of this method.

1) RECONSTRUCTION RESOLUTION OF HF ALGORITHM UNDER THE SIMULATION CONDITIONS

First of all, the HF algorithm is applied to process the υ_{sb} data along the planes where Z= −5.5mm, −9.5mm and −14.5mm i.e. υ_{sb} data are substituted into equation (9). As a result, the acoustic pressure, p_{rs} is determined and which is then compared with the COMSOL simulated acoustic pressure values given by p_s. It is shown in Fig.9, in which the continuous curves represent the calculated p_{rs} values, while the symbols o, +, and × represent the directly simulated acoustic pressure p_s values. The outputs show excellent agreement, as can be seen.

The relative errors between reconstructed (calculated) and simulation acoustic pressure data are shown in Figure 10. The green, red and blue curves in the figure represent reconstructed acoustic pressures at Z= −9.5mm, −5.5mm, and −14.5mm respectively. It can be seen that the error in the reconstructed values can be controlled with in ±0.07. The acoustic pressure reaches its maximum at the plane where Z= −9.5mm. Its reconstruction error is within ±0.01; however, two planes at Z= −9.5mm and Z= −14.5mm (where the acoustic pressures reach the minimum) have a poorer reconstruction of the values and thus a larger error. This is due to the fact that the acoustic pressure at the side boundary is ignored during the process of the reconstruction, (but in effect it is of the same order of magnitude with that of the two measured planes). As a result, the reconstruction error and the comparison between the calculated and the simulation results are relatively large.

2) EXPERIMENTAL RECONSTRUCTION EFFECT

In order to verify the precision of the acoustic pressure measured by using the LDV approach, two representative planes (at Z= −9.5 and Z= −5.5) are chosen to reconstruct the value of the acoustic pressure by using the HF algorithm, allowing then the reconstructed pressure p_e to be compared with the result of the COMSOL simulated acoustic pressure p_s.

For the convenience of comparison, the reconstructed and COMSOL simulated acoustic pressures were normalized and are shown together in figure 11(a). Here the continuous line represents the pressure reconstructed using υ_{eb} achieved from the HF algorithm, according to equation (9). The cross marks in the figure represent the data for the acoustic pressure, obtained by using the COMSOL simulation. In graph (b) of the figure, the curves illustrate the relative deviation between the reconstructed experimental and the simulated results. It can be seen that the experimental and simulated results are in good agreement, with their relative error of no more than 4%, when the maximum acoustic pressure occurs at Z = −9.5mm. However, the relative error rises to 20 % when the minimum acoustic pressure is experienced at Z= −5.5mm. As has been seen from Section 4.3.1, the HF algorithm itself has caused a reconstruction error at a value of Z= −5.5mm.

Furthermore, even if the transducer is assumed to vibrate at a particular frequency, high harmonics still occur within the acoustic field, (which arises from a nonlinear phenomenon [25]). LDV can be used to measure those harmonics

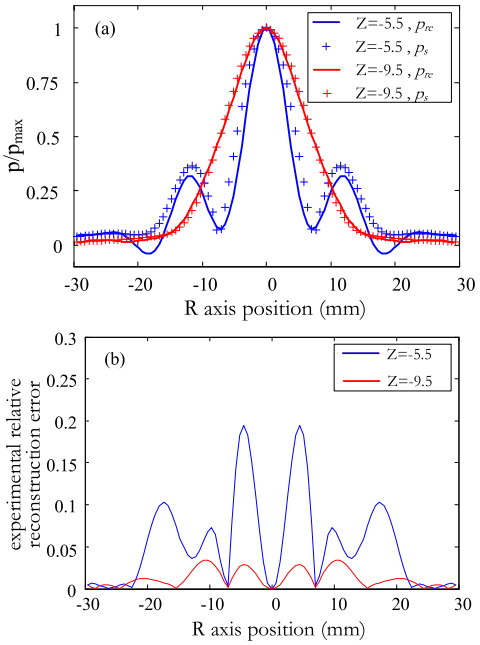

FIGURE 11. The comparison between the normalized reconstructed acoustic pressure p_{re} and COMSOL simulated p_s under the following experimental conditions: (a) is normalized acoustic pressure of simulation and experimental reconstruction and (b) is normalized reconstruction error under the experimental condition.

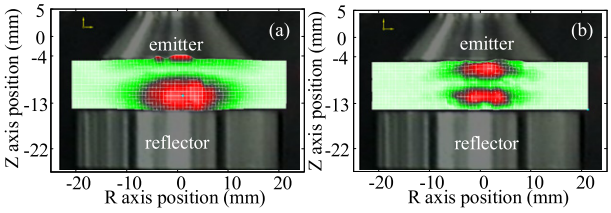

FIGURE 12. LDV output distribution of the levitation cavity at the 2nd levitation mode, (a) is fundamental frequency and (b) is the 2nd harmonic.

and Figure12 shows a comparison of the fundamental and second harmonic patterns at the second levitation mode. A further study of this will form future work.

V. CONCLUSION

LDV-based acoustic pressure measurements, targeted towards acoustic field determination has been the subject of this work. The influence of the harmonics generated in the acoustic pressure distribution has been taken into account. In summary, COMSOL-MATLAB-programming has been used to simulate υ_{sb} within the acoustic field, at the 3rd levitation mode. Then, υ_{sb} is compared with υ_{eb}, obtained using experimental methods and good agreement is obtained between the results of the simulation and those of the experiments.

Secondly, using the approach presented, the acoustic field is reconstructed at typical planes (of Z= −9.5mm and Z= −14.5mm) using MATLAB programming to obtain υ_{sb} and υ_{eb}. The reconstruction error arising in comparing the outcomes of experiment and simulation are within 7% and 20% respectively, when reconstructing the acoustic field using υ_{sb} and υ_{eb}. The method applied can also be used to realize shape recognition of non-axisymmetric acoustic fields, where only the acoustic field reconstruction algorithm is different.

ACKNOWLEDGMENT

The authors would like to thank the Simulation Center of Harbin Institute of Technology for providing LDV measurement equipment during the experiments. The support of the Royal Academy of Engineering for Grattan and Sun is appreciated.

REFERENCES

[1] T. Xu, F. Soto, W. Gao, R. Dong, V. Garcia-Gradilla, E. Magaña, X. Zhang, and J. Wang, "Reversible swarming and separation of self-propelled chemically powered nanomotors under acoustic fields," *J. Amer. Cham. Soc.*, vol. 137, no. 6, pp. 2163–2166, Jan. 2015.

[2] S. Liu, Y. Yang, T. Xie, and X. Shan, "Experimental study on fine titanium wire drawing with two ultrasonically oscillating dies," *IEEE Access*, vol. 6, pp. 16576–16587, 2018.

[3] T. Xu, F. Soto, W. Gao, V. Garcia-Gradilla, J. Li, X. Zhang, and J. Wang, "Ultrasound-modulated bubble propulsion of chemically powered microengines," *J. Amer. Cham. Soc.*, vol. 136, no. 24, pp. 8552–8555, Jun. 2014.

[4] J. Wu, Y. Mizuno, and K. Nakamura, "Polymer-based ultrasonic motors utilizing high-order vibration modes," *IEEE/ASME Trans. Mechatronics*, vol. 23, no. 2, pp. 788–799, Apr. 2018.

[5] L. Zhang, X. Shan, X. Zhang, and T. Xie, "A method for reducing the drag of the ship shaped wall by using piezoelectric ceramic vibrators," *IEEE Access*, vol. 7, pp. 13295–13303, 2019.

[6] R. J. Olive, W. H. Hofmeister, R. J. Bayuzick, G. Carro, J. P. McHugh, R. H. Hopkins, M. Vlasse, J. K. R. Weber, P. C. Nordine, and M. McElfresh, "Formation of tetragonal $YBa_2Cu_3O_7$-δ from an undercooled melt," *J. Mater. Res.*, vol. 9, no. 1, pp. 1–3, Jan. 1994.

[7] S. Bauerecker and B. Neidhart, "Formation and growth of ice particles in stationary ultrasonic fields," *J. Chem. Phys.*, vol. 109, no. 10, pp. 3709–3712, Sep. 1998.

[8] J. R. Gao, C. D. Cao, and B. Wei, "Containerless processing of materials by acoustic levitation," *Adv. Space Res.*, vol. 24, no. 10, pp. 1293–1297, 1999.

[9] A. Scheeline and R. L. Behrens, "Potential of levitated drops to serve as microreactors for biophysical measurements," *Biophys. Chem.*, vols. 165–166, pp. 1–12, May 2012.

[10] R. J. Weber, C. J. Benmore, S. K. Tumber, A. N. Tailor, C. A. Rey, L. S. Taylor, and S. R. Byrn,, "Acoustic levitation: Recent developments and emerging opportunities in biomaterials research," *Eur. Biophys. J.*, vol. 41, no. 4, pp. 397–403, Apr. 2012.

[11] M. Sundvik, H. J. Nieminen, A. Salmi, P. Panula, and E. Hæggström, "Effects of acoustic levitation on the development of zebrafish, danio rerio, embryos," *Sci. Rep.*, vol. 5, Sep. 2015, Art. no. 13596.

[12] H. Wang, S. Mu, F. Zhang, H. Wang, H. Liu, H. Zhang, and X. Kang, "Effects of atrazine on the development of neural system of zebrafish, danio rerio," *Biomed. Res. Int.*, vol. 2015, Apr. 2015, Art. no. 976068.

[13] T. Vasileiou, D. Foresti, A. Bayram, D. Poulikakos, and A. Ferrari, "Toward contactless biology: Acoustophoretic DNA transfection," *Sci. Rep.*, vol. 6, Feb. 2016, Art. no. 20023.

[14] M. Petersson, J. Nilsson, L. Wallman, T. Laurell, J. Johansson, and S. Nilsson, "Sample enrichment in a single levitated droplet for capillary electrophoresis," *J. Chromatogr. B, Biomed. Sci. Appl.*, vol. 714, no. 1, pp. 39–46, Aug. 19s98.

[15] J. Leiterer, F. Delissen, F. Emmerling, A. F. Thünemann, and U. Panne, "Structure analysis using acoustically levitated droplets," *Anal. Bioanal. Chem.*, vol. 391, no. 4, pp. 1221–1228, Jun. 2008.

[16] A. M. Seddon, S. J. Richardson, K. Rastogi, T. S. Plivelic, A. M. Squires, and C. Pfrang, "Control of nanomaterial self-assembly in ultrasonically levitated droplets," *J. Phys. Chem. Lett.*, vol. 7, no. 7, pp. 1341–1345, Mar. 2016.

[17] D. Zang, Z. Chen, and X. Geng, "Sectorial oscillation of acoustically levitated nanoparticle-coated droplet," *Appl. Phys. Lett.*, vol. 108, no. 3, Jan. 2016, Art. no. 031603.
[18] H. L. Cao, D. C. Yin, Y. Z. Guo, X. L. Ma, J. He, W. H. Guo, X. Z. Xie, and B. R. Zhou, "Rapid crystallization from acoustically levitated droplets," *J. Acoust. Soc. Amer.*, vol. 131, no. 4, pp. 3164–3172, Apr. 2012.
[19] Y. Ochiai, T. Hoshi, and J. Rekimoto, "Pixie dust: Graphics generated by levitated and animated objects in computational acoustic-potential field," *ACM Trans. Graph.*, vol. 33, no. 4, Jul. 2014, Art. no. 85.
[20] Y. Wang, P. Theobald, J. Tyrer, and P. Lepper, "The application of scanning vibrometer in mapping ultrasound fields," *J. Phys., Conf. Series*, vol. 1, no. 1, pp. 167–173, 2004.
[21] L. Chen, S. J. Rupitsch, and R. Lerch, "A reliability study of light refractive tomography utilized for noninvasive measurement of ultrasound pressure fields," *IEEE Trans. Ultrason., Ferroelectr., Freq. Control*, vol. 59, no. 5, pp. 915–927, May 2012.
[22] L. Chen, S. J. Rupitsch, and R. Lerch, "Noninvasive measurement of time-dependent ultrasound fields in different materials," in *Proc. IEEE Int. Ultrason. Symp.*, Dresden, Germany, Oct. 2012, pp. 2176–2179.
[23] K. Nakamura, "Sound field measurement through the acousto-optic effect of air by using laser Doppler velocimeter," in *Proc. 4th Pacific Rim Conf. Lasers Electro-Opt.*, Jul. 2001, pp. 154–155.
[24] D. Koyama and K. Nakamura, "Noncontact ultrasonic transportation of small objects in a circular trajectory in air by flexural vibrations of a circular disc," *IEEE Trans. Ultrason., Ferroelectr., Freq. Control*, vol. 57, no. 6, pp. 1434–1442, Jun. 2010.
[25] M. A. B. Andrade, T. S. Ramos, F. T. A. Okina, and J. C. Adamowski, "Nonlinear characterization of a single-axis acoustic levitator," *Rev. Sci. Instrum.*, vol. 85, no. 4, Apr. 2014, Art. no. 045125.
[26] M. A. Andrade, N. Pérez, and J. C. Adamowski, "Experimental study of the oscillation of spheres in an acoustic levitator," *J. Acoust. Soc. Amer.*, vol. 136, no. 4, pp. 1518–1529, Oct. 2014.
[27] N. Pérez, M. A. Andrade, R. Canetti, and J. C. Adamowski, "Experimental determination of the dynamics of an acoustically levitated sphere," *J. Appl. Phys.*, vol. 116, no. 18, Nov. 2014, Art. no. 184903.
[28] A. Torras-Rosell, S. Barrera-Figueroa, and F. Jacobsen, "Sound field reconstruction using acousto-optic tomography," *J. Acoust. Soc. Amer.*, vol. 13, pp. 3786–3793, May 2012.
[29] E. F. Grande, A. T. Rosell, and F. Jacobsen, "Holographic reconstruction of sound fields based on the acousto-optic effect," in *Proc. 42nd Int. Congr. Expo. Noise Control Eng.*, Sep. 2013, vol. 247, no. 5, pp. 3181–3190.
[30] T. R. Antoni and B. F. Salvador, "An acousto-optic method for free-field microphone calibration," in *Proc. ICSV*, Florence, Italy, vol. 22, 2015, pp. 1–8.
[31] K. Ishikawa, K. Yatabe, N. Chitanont, Y. Ikeda, Y. Oikawa, T. Onuma, H. Niwa, and M. Yoshii, "High-speed imaging of sound using parallel phase-shifting interferometry," *Opt. Express*, vol. 24, no. 12, pp. 12922–12932, 2016.
[32] D. C. Williams, *Optical Methods in Engineering Metrology*. London, U.K.: Chapman & Hall, 1993.
[33] L. Bahr and R. Lerch, "Beam profile measurements using light refractive tomography," *IEEE Trans. Ultrason., Ferroelectr., Freq. Control*, vol. 55, no. 2, pp. 405–413, Feb. 2008.
[34] R. Bracewell, *The Fourier Transform and Its Applications*, 3rd ed. New York, NY, USA: McGraw-Hill, 2000.

HUIJUAN DONG was born in Henan, China, in 1968. She received the B.E. degree in precise mechanical engineering and the master's and Ph.D. degrees in mechatronics engineering from the Harbin Institute of Technology, in 1990, 1996, and 1999, respectively, where she joined in 1997. Subsequently, she was promoted to an Associate Professor in 2001, and a Full Professor in 2012. Her research project focuses on acoustics.

ZHEN YU was born in Heilongjiang, China, in 1993. He received the B.E. and M.E. degrees in mechatronics engineering from the School of Mechanical Engineering, Harbin Institute of Technology, in 2015 and 2017, respectively. His research interests include ultrasonic vibration and industrial robots and control.

KENNETH THOMAS VICTOR GRATTAN was born in Lurgan, U.K., in 1953. He received the B.Sc. degree (Hons.) in physics and the Ph.D. degree in laser physics from Queen's University Belfast, in 1974. He became a Research Fellow of the Imperial College of Science and Technology, in 1978. In 1983, he joined the City University of London as a new blood Lecturer in physics being appointed as a Professor of measurement and instrumentation, in 1991, and the Head of the Department of Electrical, Electronic, and Information Engineering. From 2001 to 2008, he was the Associate and then the Deputy Dean of the School of Engineering, from 2008 to 2012, and the first Conjoint Dean of the School of Engineering and Mathematical Sciences and the School of Informatics. In 2013, he was appointed as the Inaugural Dean of the City Graduate School. He was appointed as a George Daniels Professor of scientific instrumentation, in 2013, and the Royal Academy of Engineering Research Chair, in 2014. He was elected to the Royal Academy of Engineering, the U.K. National Academy of Engineering, in 2008. His research interests have expanded to the measurement of a range of physical and chemical parameters using optical methods.

TONG SUN was born in Jiangsu, China, in 1968. She received the B.E., M.E., and D.Eng. degrees from the Department of Precision Instrumentation, Harbin Institute of Technology, Harbin, China, in 1990, 1993, and 1998, respectively, and the Ph.D. degree in applied physics from City University, in 1999. She was an Assistant Professor with Nanyang Technological University, Singapore, from 2000 to 2001, before she re-joined the City University of London, in 2001, as a Lecturer. Subsequently, she was promoted to a Senior Lecturer, in 2003, a Reader, in 2006, and a Professor, in 2008, with the City University of London. Her research project focuses on developing a range of optical fiber sensors.

TIANLONG LI was born in Jilin, China, in 1988. He received the B.E. degree from the School of Mechanical Engineering, Harbin Institute of Technology, in 2010, and the M.E. and Ph.D. degrees in mechatronics engineering from the Harbin Institute of Technology, in 2012 and 2017, respectively. From 2017 to 2018, he was an Assistant Professor with the School of Mechanical Engineering, Harbin Institute of Technology, where he has been an Associate Professor with the State Key Laboratory of Robotics and System, since 2018. He was also a Foreign Professor with the Institute of Pharmacy, Sechenov University. His research project focuses on micro-/nanorobots.